2012

Numerical Analysis of Performance, Rotor Temperature Distributions, and Rotor Thermal Deformation of an R134a Screw Compressor

Shenghung Hsieh
imewhh@ccu.edu.tw

Wenhsin Hsieh

Chishun Huang

Yuhua Huang

Point-to-point reply to reviewer's comments

Comment 1:
Please use title case in the paper title (the first letter of each word should be uppercase unless the word is a preposition, conjunction, or article). For example Numerical Analysis of Performance, Rotor Temperature Distributions, and Rotor Thermal Deformation of an R134a Screw Compressor).

Reply:
The authors have used title case in the paper title, as shown in **Page 1** of the revised manuscript.

Comment 2:
Please give family names of the authors in ALL CAPITAL letters (Sheng-hung HSIEH, Wen-Hsin HSIEH, Chi-Shun HUANG, Yu-Hua HUANG).

Reply:
The authors have given family names of the authors in all capital letters, as shown in **Page 1** of the revised manuscript.

Comment 3:
Please remove the hyperlink in the corresponding author email address (the font should be black without underline).

Reply:
The authors have removed the hyperlink in the corresponding author email address, as shown in **Page 1** of the revised manuscript.

Comment 4:
Please do not indent the first line of paragraphs, but leave a blank line between paragraphs. This may require some minor editing to stay within the page limit.

Reply:
According to this comment, the authors have corrected the format of manuscript, as shown in the revised manuscript.

Comment 5:
Color-coded plots such as those in Figures 7-10 may be easier to read in black and white if a gray scale rather than a color spectrum scale is used. This is left to the discretion of the authors.

Reply:
After comparing the Figures 7-10 shown by gray scale and the color spectrum scale, the authors think that the ones shown by color spectrum scale could be read more clearly. Therefore, the authors decide to use the color spectrum plots of Figures 7-10 in **Page 8** of the revised manuscript.

Comment 6:
Please remove the hyperlink in the COMSOL entry of the References section (the font for the website should be black without underline).

Reply:
The authors have removed the hyperlink in the COMSOL entry of the References section, as shown in **Page 10** of the revised manuscript.

Numerical Analysis of Performance, Rotor Temperature Distributions, and Rotor Thermal Deformation of an R134a Screw Compressor

Sheng-hung HSIEH[1], Wen-Hsin HSIEH[1]*, Chi-Shun HUANG[2], Yu-Hua HUANG[2]

[1] Department of Mechanical Engineering and Advanced Institute of Manufacturing for High-Tech Innovations, National Chung Cheng University, Chia-Yi, Taiwan, R.O.C.

[2] Hanbell Precise Machinery Co., Tao-Yuan Hsien, Taiwan, R.O.C.
TEL: +886-3-4836215
E-mail: sales@hanbell.com

* Corresponding Author
Tel: +886-5-2428170
Fax: +886-5-2720589
Email: imewhh@ccu.edu.tw

ABSTRACT

A numerical analysis is performed to systematically calculate the performance, rotor temperature distributions, and rotor thermal deformation of an R134a screw compressor. The analysis procedure includes three major steps. The first step calculates the efficiencies and the temperature- and pressure-time histories of the refrigerant during a compression cycle of the screw compressor. The calculation is performed based on a theoretical model, which considers the mass and energy conservation laws, the leakages through various paths, and the discharges of gas and oil. The heat transfer between gas and oil is also considered. The second step calculates the temperature distributions in the rotors by numerically solving the set of Helmholtz equations derived from the partial differential equations for transient heat conduction of the rotors. Each of the two rotors is subject to a periodic convective boundary condition and five steady boundary conditions. The third step calculates thermal deformations of rotors by a finite element method based on the calculated temperature distributions from the second step. The proposed theoretical models and numerical procedures are shown to be able to efficiently calculate the performance, rotor temperature distributions, and rotor thermal deformations. The calculated information is important and useful in the design of a refrigerant screw compressor.

1. INTRODUCTION

In a refrigeration system, a compressor is used to increase the pressure of gaseous refrigerant. The refrigerant screw compressor, compared with other types of compressors, is constructed with fewer parts and therefore is more reliable. The rotational operation of the rotors also provides better characteristics of dynamic balance. In addition, the exhaust flow rate is not affected by the discharge pressure due to the forced transportation mechanism used in screw compressors. Due to the above-mentioned advantages, the screw compressor is widely used in many industrial applications, in addition to refrigeration systems.

When designing a refrigerant screw compressor, it is important to optimize the performance of the screw compressor in consideration of physical properties of refrigerants. The design work can be efficiently carried out by numerical design tools for the compressor geometry, analysis of thermo-fluidic compression processes and calculation of screw deformations caused by thermal and mechanical loads. In recent years, the development of numerical design tools has attracted attention of many researchers. The numerical design tool for compressor geometry has been used to design the screw profiles in consideration of the gear theory, performance of the screw compressor, and loadings on the rotors (Stosic, et al. 2005, Wu, et al. 2008, Xing 2000). The shapes of the case, inlet port, and outlet port, the

detailed information on the volume of compression chamber and the areas of the inlet port, outlet port, and leakage paths are also obtained by the numerical design tool.

The numerical design tools for analyzing the compressor performance and thermo-fluidic processes could be separated into two categories: lumped parameter analysis and computational fluid dynamics (CFD) analysis. In lumped parameter analysis (Fleming, et al. 1998, Fujiwara, et al. 1995, Hsieh, et al. 2011, Seshaiah, et al. 2007, Stosic, et al. 1990, Wu, et al. 2004), the properties of the compressed refrigerant inside the compression chamber are considered to be uniform, but time dependent, and their changes are described by the conservation of mass and energy. The calculated volumetric efficiency, isentropic efficiency, and pressure curve are verified by experimental results. In CFD analysis (Kovacevic 2005, Kovacevic, et al. 2007, Kovacevic, et al. 2007), the transient, three dimensional thermo-fluidic model was proposed and solved by commercial programs to calculate the properties of the compressed refrigerant inside the compression chamber. The results were further used in the solid-fluid coupled model to calculate the deformation of rotors. The detailed phenomena, such as the flow fields, the temperature distribution, and the thermal deformation in the rotors, are available to the designers. The computation is, however, usually very long.

The numerical design tools for calculating the deformations of the screws caused by thermal and mechanical loads were proposed in the past (Gao, et al. 2011, Hsieh, et al. 2011, Kovacevic, et al. 2007, Lee, et al. 1999, Stosic, et al. 2005). Stosic et al. (Stosic, et al. 2005) and Lee et al. (Lee, et al. 1999) used the calculated properties of the compressed medium, which were obtained by a lumped parameter analysis, to calculate the average axial radial forces exerted on the bearing. Hsieh et al. (Hsieh, et al. 2011) also used the calculated properties of the compressed medium from a lumped parameter analysis, and introduced the auxiliary complex equation (ACE) method to calculate the temperature distribution in the rotors. The calculated temperature distributions in the rotors were used to estimate the approximate thermal deformation of the screws. Considering the forces exerted on rotors and temperature effects, Kovacevic et al. (Kovacevic, et al. 2007) and Gao et al. (Gao, et al. 2011) performed an thermal and dynamic deformation analysis of the rotors by finite element method (FEM).

Table 1: Design parameters and operating conditions

Parameters	Male screw	Female screw
Number of teeth	5	6
Outer diameter (mm)	174	139
Length of screw (mm)	164	164
Lead ($mm/360^o$)	228	273.6
Clearance of the inlet end of the screw (mm)	0.25	0.25
Clearance of the outlet end of the screw (mm)	0.05	0.05
Clearance of the sealing line of the screw (mm)	0.08	0.08
Clearance between rotors (mm)	0.03	0.03
Type of refrigerant	R134a	
Rotation speed (rpm)	3550	
Inlet pressure (MPa)	0.36	
Outlet pressure (MPa)	0.93	

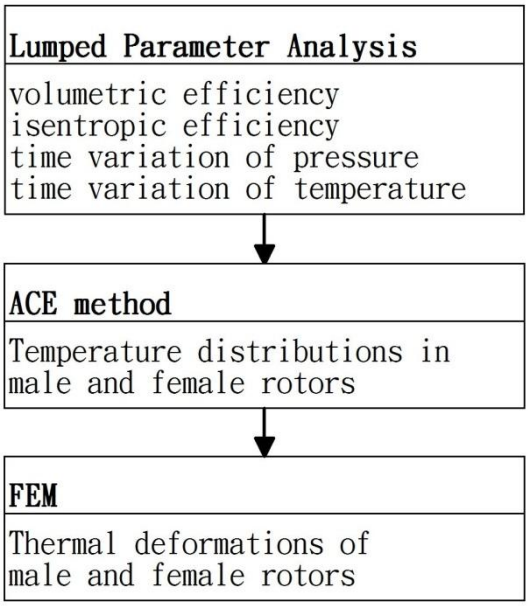

Figure 1: The numerical procedure used in this study

In these above-mentioned numerical design tools, each tool can provide certain accurate and useful design information for designers. But these tools have not yet been completely integrated to efficiently calculate the performance, rotor temperature distributions, and rotor thermal deformations of a refrigerant screw compressor. In this paper, theoretical models and numerical procedures are proposed to efficiently calculate the performance, rotor temperature distributions, and rotor thermal deformations. The numerical procedure includes three major steps. The

first step calculates the efficiencies and the temperature- and pressure-time histories of the refrigerant during a compression cycle of the screw compressor. The second step calculates the rotor temperature distributions by numerically solving the set of Helmholtz equations derived from the partial differential equations for transient heat conduction of the rotors. The third step calculates rotor thermal deformations by a finite element method based on the calculated rotor temperature distributions from the second process.

2. Theoretical models and numerical procedures

In this study, numerical design tools are established and integrated to calculate the compressor performance, rotor temperature distributions, and rotor thermal deformations of a commercial refrigerant screw compressor (RC2-410A, Hanbell Precise Machinery Co., Ltd), which operates steadily under the condition listed in Table 1. Table 1 also shows the design parameters of the employed compressor. The numerical design tools include lumped parameter analysis for calculating properties of compressed refrigerant, ACE method, for temperature distributions in male and female rotors, and FEM, for thermal deformations of male and female rotors. The numerical procedures are shown in Figure1. In the first step, the lumped parameter analysis is implemented to calculate the volumetric and isentropic efficiencies and time variations of pressure and temperature of the compressed refrigerant. The calculated results are then used in the second step, in which the transient three-dimensional heat conduction equation subjected to periodic boundary condition without internal heat generation is solved by the ACE method. The calculated rotor temperature distributions are used in the third step, in which the commercial FEM program, COMSOL Multiphysics (COMSOL), is used to calculate thermal deformation of male and female rotors. These numerical procedures are completely integrated to efficiently calculate the performance, rotor temperature distributions, and rotor thermal deformations of a refrigerant screw compressor. The theoretical models adopted in the numerical procedures are shown in the following paragraphs.

2.1 Compressor performance

The lumped parameter analysis of this study considers a deformable control volume that represents one of the compression chambers of a refrigerant screw compressor, as shown in Figure 2. The compression chamber is filled with refrigerant and injected with oil. The model considers the equations of the conservation of mass and energy for the refrigerant and the oil and the equation of state for the refrigerant. The entrance of the refrigerant, injection of the oil, reinjection of the refrigerant, discharges of the refrigerant and the oil and leakages through the contact line, sealing line, blow hole and ends of screws are considered on the boundary of the control volume. Within the control volume the heat transfer between the refrigerant and the oil drops and that between the refrigerant and the oil film are also included in the model.

The four ordinary differential equations (ODEs) used in the lumped parameter analysis are the mass conservation equation for the refrigerant, Equation (1), the mass conservation equation for the oil, Equation (2), the energy equation for the refrigerant, Equation (3), and the energy equation for the oil, Equation (4).

$$\omega \frac{dm_{ref}}{d\theta} = \dot{m}_{ref,ent} + \dot{m}_{ref,dis} + \dot{m}_{ref,leakage} \tag{1}$$

$$\omega \frac{dm_{oil}}{d\theta} = \dot{m}_{oil,inj} + \dot{m}_{oil,dis} + \dot{m}_{oil,leakage} \tag{2}$$

$$\omega \frac{dU_{ref}}{d\theta} = \dot{H}_{ref,ent} + \dot{H}_{ref,dis} + \dot{H}_{ref,leakage} + \dot{H}_{ref,reinjection} - \dot{Q}_{ref-oil} - \dot{W}_{ref} \tag{3}$$

$$\omega \frac{dU_{oil}}{d\theta} = \dot{H}_{oil,inj} + \dot{H}_{oil,dis} + \dot{H}_{oil,leakage} + \dot{Q}_{ref-oil} \tag{4}$$

In order to calculate mass flow rate of leakages, which were clearly classified by Fleming et al. (Fleming, et al. 1995), the equation for isentropic flow is used to calculate the flow velocity, as shown in Equation (5). This equation can be used in calculating the mass flow rate of leakage of screw compressor (Hsieh, et al. 2011). In Equation (5), ξ is the empirical constant for calculating the mass flow rate. Since there are four kinds of leakage, the mass flow rate of leakage through the blow hole is calculated by ξ_{blow}, the one through the sealing line by $\xi_{sealing}$, the one through the ends of the screws by ξ_{end}, and the one through the contact line by $\xi_{contact}$. For calculating the mass flow rate of discharge, the Equation (6), is used to consider the two effects of the pressure difference across the outlet and the axial velocity of the refrigerant (Hsieh, et al. 2011).

$$\dot{m}_{ref} = \xi \cdot A \cdot \rho_{ref} \cdot V \tag{5}$$

$$V = V_{sound} \quad \text{when the ratio of upstream to downstream pressures} \le \beta^*$$
$$V = Ma_{th} \cdot V_{sound} \quad \text{when the ratio of upstream to downstream pressures} > \beta^*$$
$$\beta^* = (2/k+1)^{k/(k-1)}$$
$$\dot{m}_{mix} = A_{dis} \cdot \rho_{mix} \cdot \sqrt{\xi_p \cdot 2k/\rho_{mix}(k-1) \cdot \Delta p + \xi_{sv} \cdot (\omega \cdot Lead)^2} \quad (6)$$

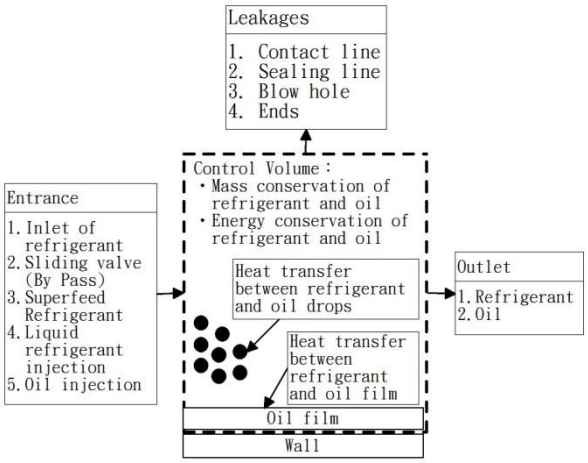

Figure 2: The physical model of lumped parameter analysis

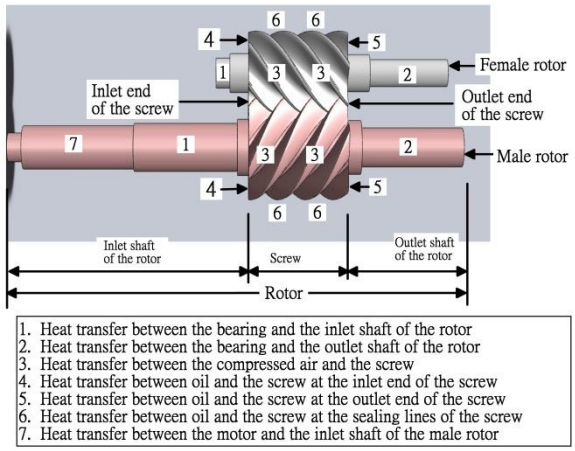

Figure 3: The heat-transfer model of male and female rotors

To calculate the heat transfers between refrigerant and oil, Equations (7) and (8) are used to calculate the heat transfer between refrigerant and oil drops (Fleming, et al. 1998, Hsieh, et al. 2011, Li, et al. 2009, Stosic, et al. 1992, Wu, et al. 2004, Zamfirescu, et al. 2004). Equations (9) and (10) are used to calculate the heat transfer between refrigerant and oil film (Fujiwara, et al. 1995, Hsieh, et al. 2011, Zamfirescu, et al. 2004).

$$\dot{Q} = \xi_{heat} h_{oil\ drop} A_{oil\ drop} (T_{ref} - T_{oil}) \quad (7)$$
$$h_{oil\ drop} = N_u \cdot \lambda_{oil} / D_{oil\ drop} \quad (8)$$
$$N_u = 2 + 0.6 Re^{0.5} Pr^{0.33}$$
$$\dot{Q} = \xi_{heat} h_{oil\ film} V_c^{2/3} (T_{ref} - T_{oil}) \quad (9)$$
$$h_{oil\ film} = N_u \lambda / D_{male} \quad (10)$$
$$N_u = 0.51 Re_\omega^{0.74}$$
$$Re_\omega = \omega D_{male}^2 / \mu$$

2.2 Rotor temperature distributions

The heat-transfer model of male and female rotors is shown in Figure 3. When the screw compressor operates steadily, the temperature distributions in the male and female rotors are affected by seven heat-transfer boundary conditions, which are shown schematically in Figure 3. The first one is the heat transfer between the rotor and the bearing at the inlet shaft of the rotor. The second one is the heat transfer between the rotor and the bearing at the outlet shaft of the rotor. The third one is the convective heat transfer between the screw and the compressed air. The forth one is the heat transfer between the screw and oil at the inlet end of the screw. The fifth one is the heat transfer between the screw and oil at the outlet end of the screw. The sixth one is the heat transfer between the screw and oil at the sealing line. The seventh one is the heat transfer between the motor and the inlet shaft of the male rotor.

In this study, the rotor temperature distributions are solved by the ACE method (Hsieh, et al. 2011), in which the Helmholtz equations are used to describe a boundary-value problem involving a periodic boundary condition. There are three advantages of calculating the temperature in the rotor by solving the Helmholtz equations and associated boundary conditions [Equations (11) – (15) given below]. The first is that the solution is independent of the initial condition of temperature. The second is that the original time-dependent three-dimensional system is converted to a time-independent three dimensional system. This reduces significantly the computation time. The third is that the temperature at any time during a cycle can be efficiently obtained by Equations (14) and (15), without the use of interpolation, which usually increases the calculation time.

$$\nabla^2\psi_m - \frac{i\cdot\omega_m}{\alpha}\psi_m = 0 \tag{11}$$

$$\lambda_2\frac{\partial\psi_m}{\partial n} = h\cdot\left(A_{m,ref} - \psi_m\right) \tag{12}$$

$$\lambda_2\frac{\partial\psi_m}{\partial n} = \dot{q}_a,\quad a = 1,\dots,6,\quad \text{when } m \neq 0,\ q_a = 0 \tag{13}$$

$$T_d = \sum_{m=0}^{\infty}\psi_m\cdot exp(\mathrm{i}\cdot\omega_m\cdot\tau) \tag{14}$$

$$where\ \ \tau = rem(t, t_p)$$

$$T_r = Re(T_d) \tag{15}$$

In Equation (12), the convective heat-transfer coefficient h is calculated as the product of an empirical constant ξ_{ref} and an ideal convective heat-transfer coefficient h_{ideal}, as shown in Equations (16) – (19). The empirical constant ξ_{ref} represents the ratio of the actual to the ideal convective heat-transfer coefficients.

$$Nu_D = \frac{(f/8)(Re_D-1000)Pr}{1+12.7(f/8)^{1/2}\left(Pr^{2/3}-1\right)}\left[1+\left(\frac{D_H}{L}\right)^{2/3}\right] \tag{16}$$

$$5000 < Re_D < 10^8, 100 < D_H/\varepsilon < 10^6$$

$$h_{ideal} = Nu_D\cdot\lambda/D_H \tag{17}$$

$$h = \xi_{ref}\cdot h_{ideal} \tag{18}$$

$$f = 0.25/[log(1/(3.7D_H/\varepsilon) + 5.74/Re_D^{0.9})]^2 \tag{19}$$

The ideal heat fluxes from the oil to the screw at the sealing line, inlet end of the screw and outlet end of the screw are calculated by the formulas given by Xing (Xing 2000). The ideal heat flux at the sealing line is calculated by Equation (20) and the actual heat flux, Equation (21). The ideal heat fluxes from oil to the screw at the inlet and outlet ends of the screw are respectively calculated by Equations (22) and (24). The actual heat fluxes are calculated by Equations (23) and (25).

$$\dot{q}_{of,ideal} = \mu\omega^2 D_o^2/\left(4\delta_f\right) \tag{20}$$

$$\dot{q}_{of} = \xi_{of}\cdot\dot{q}_{of,ideal} \tag{21}$$

$$\dot{q}_{os,ideal} = \mu\omega^2 r^2/\delta_s \tag{22}$$

$$\dot{q}_{os} = \xi_{os}\cdot\dot{q}_{os,ideal} \tag{23}$$

$$\dot{q}_{od,ideal} = \mu\omega^2 r^2/\delta_d \tag{24}$$

$$\dot{q}_{od} = \xi_{od}\cdot\dot{q}_{od,ideal} \tag{25}$$

The ideal heat flux from a bearing to the rotor shaft is determined by dividing the bearing power loss by the area of the bearing. The ideal bearing power loss is calculated by Equation (26) (Tedric, et al. 2006).The torque (M_l) due to the applied load is calculated by Equation (27). The torque (M_v) due to lubricant viscous friction is calculated by Equation (28) (Jeng, et al. 2003). The torque (M_f) due to roller end-ring flange sliding friction for a roller bearing is calculated by Equation (29). The actual conductive heat fluxes from the bearing located at the inlet and outlet shafts of the rotor are respectively calculated by Equations (30) and (31).

$$\dot{Q}_{b,\,ideal} = 0.001\times\omega\times M \tag{26}$$

$$M = \begin{cases} M_l + M_v & for\ the\ ball\ bearing \\ M_l + M_v + M_f & for\ the\ roller\ bearing \end{cases}$$

$$M_l = f_l\cdot d_m\cdot F_\gamma \tag{27}$$

$$\text{where} f_l = \begin{cases} 0.00028 & for\ the\ ball\ bearing \\ 0.0015 & for\ the\ roller\ bearing \end{cases}$$

$$M_v = 2.29\times10^{-16}\cdot f_o\cdot(\nu_o\cdot 2\pi\cdot\omega)^2\cdot d_m^3 \tag{28}$$

$$\text{where} f_o = \begin{cases} 6.6 & for\ the\ ball\ bearing \\ 8 & for\ the\ roller\ bearing \end{cases}$$

$$M_f = 0.006\cdot F_{axial}\cdot d_m \tag{29}$$

$$q_{bs} = \xi_{bs} \cdot Q_{bs,\,ideal} / A_{bs} \tag{30}$$

$$q_{bd} = \xi_{bd} \cdot Q_{bs,\,ideal} / A_{bd} \tag{31}$$

2.3 Rotor thermal deformations

In this study, the calculated rotor temperature distributions are used in thermal deformation analysis. The thermal deformations in male and female rotors are obtained by solving Equation (32) with the commercial program (COMSOL Multiphysics). The reference temperature is 25 ℃. The boundary conditions of zero axial and radial displacements are imposed on the two interfaces between the outlet shafts of the male and female rotors and the bearings. On the other hand, the boundary conditions of zero radial displacement are imposed on the two interfaces between the inlet shafts of the male and female rotors and the bearings.

$$\epsilon_{th} = \begin{bmatrix} \epsilon_x \\ \epsilon_y \\ \epsilon_z \\ \gamma_{xy} \\ \gamma_{yz} \\ \gamma_{xz} \end{bmatrix}_{th} = \alpha_{th}\left(T_r - T_{reference}\right) \tag{32}$$

3. Results and Discussion

The above mentioned theoretical model and numerical procedure are used to calculate the compressor performance, rotor temperature distributions, and rotor thermal deformations. The calculated pressure- and temperature-time histories of refrigerant during a compression cycle are shown in Figure 4. Figure 4 shows that the pressure and temperature of refrigerant are steady during the suction process (less than the angle of 365 degrees). During the compression process (between angles of 365 to 560 degrees), the refrigerant pressure and temperature increase monotonically due to the compression. When the outlet port is just opened (at the angle of 560 degrees), the area of outlet port is still small and consequently, the resistance to gas flow through the outlet port is large. Thus, the gas pressure continues to increase and the first pressure peak appears near the angle of 577 degrees. The first pressure peak in the compression chamber begins to diminish when the outlet port area is large enough to relieve the pressure. The pressure in the compression chamber then maintains at a constant level until the second peak appears near the angle of 687 degrees. The second pressure peak is caused by the fact that the opening area of the outlet port is small and the following compression chambers are also in the discharge process.

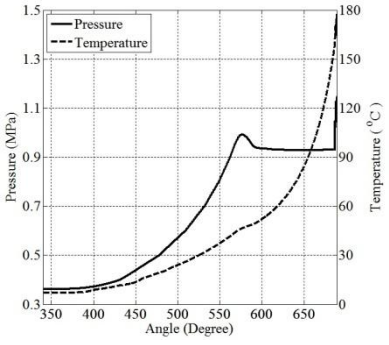

Figure 4: The calculated refrigerant pressure- and temperature-time histories during a compression cycle

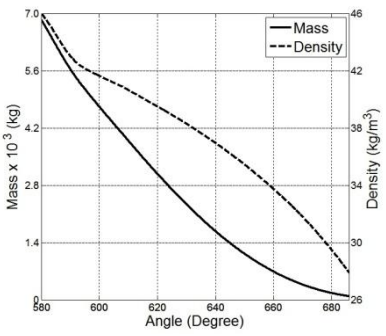

Figure 5: The calculated refrigerant mass- and density-time histories during the discharge process

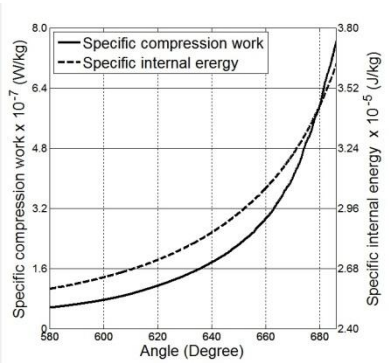

Figure 6: The calculated refrigerant specific compression work- and specific internal energy-time histories during the discharge process

Figure 5 shows the calculated refrigerant mass- and density-time histories during the discharge process. During the discharge process, the mass of refrigerant in the compression chamber and the volume of the compression chamber

are both decreased. The decreasing rate of the mass of refrigerant is larger than that of the volume of the compression chamber. This results in the decreased density of refrigerant in the compression chamber, as shown in Figure 5. Figure 6 shows that the specific internal energy of refrigerant, which is affected by the compression work, mass transfer and heat transfer, increases continuously during the discharge process. The increase in the specific internal energy during the discharge process is due to the combined effect of the increased specific compression work (shown in Figure 6) and the decreased refrigerant mass in the compression chamber (shown in Figure 5). As a result of the increase in the specific internal energy, the temperature also increases monotonically during the discharge process as shown in Figure 4.

The calculated refrigerant pressure shown above is used to calculate the axial and radial forces exerted on bearings. The heat generated by the bearings is then obtained. The calculated refrigerant temperature shown above is used to calculate the heat transfer between refrigerant and rotor. With these calculated forces, heat generation and heat transfer, we can then calculate the rotor temperature distributions. The calculated rotor temperature distributions are shown in Figure 7. Figure 7 shows the isotherm graphs at the three cross sections of the male and female rotors [(a) 0.01 m from the inlet end, (b) 0.08 m from the inlet end, and (c) 0.15 m from the inlet end]. Near the inlet end of the screw, the temperature distributes uniformly in the male and female screws, as shown in Figure 7(a). The temperature at the center of the screw is only slightly higher than that at the surface. In the middle of the screw, Figure 7(b) shows that the temperature distributes uniformly in the regions bounded by the root circles of the male and female screws. Lower temperatures exit in the area near the back flank of the male screw and in the area between the back flank and the top land of the female screw. Figure 7(c) shows the temperature distribution on the cross sections close to the outlet end of the screw. It is noted that the temperature at the center is the highest in the cross section of each of the male and female screws. This indicates that heat is transferred radially from the center to the surface of the screw and is taken away by the force convection of the compressed air at the surface of the screw. A comparison of Figure 7(a) with Figures 7(b) and 7(c) reveals that the temperature difference between the center and the surface of the screw on the cross section near the outlet end is larger than those on the other two cross sections. This indicates that the heat transferred radially from the center to the surface of the screw is larger at the section near the outlet end than that at the other two cross sections that are located at the middle and inlet end. This is probable due to the fact the bearing located at the outlet end of the rotor generates most heat.

In order to investigate the effect of the heat generated by the bearings on the rotor temperature distributions, a parametric study is conducted in this work. In the parametric study, the heat generation from the bearings is systematically changed from 90%, 100% to 110% of the baseline condition. The baseline condition is the test condition shown in Figure 7. Figures 8 and 9 are the calculated rotor temperature distributions at 110% and 90% heat generation from the bearings of the baseline condition, respectively. In comparison of Figures 7 to 9, it is evident that the rotors temperature is raised by increasing the heat generation from the bearings. In Figure 9(c), the maximum temperature difference between the center and the surface of the screw is larger than the ones in Figures 7(c) and 8(c). This implies that the increase in the heat generation form the bearings promotes the radial heat transfer in the screw. These two observations show that the calculated rotor temperature distributions are affected by the heat generation from the bearings. In order to obtain accurate rotor temperature distributions, the heat generated by the bearings need to be accurately verified by experimental results.

In this study, the rotor temperature distributions are used to calculate rotor thermal deformations. The calculate rotor thermal deformations are shown in Figure 10. Due to that the temperature of the male and female rotors is larger than the room temperature (shown in Figure 7), both the male and female rotors expand in the radial and axial directions, as shown in Figure10. Figure 10 (a) shows that the rotors expand axially toward the inlet side of rotors. Because of the boundary conditions of zero axial and radial displacements applied to the surfaces of outlet shafts of rotors, the axial thermal expansion only happens in the direction toward the inlet side of rotors. The axial displacements on the inlet ends of screws are about 8 μm. Figure 10 (b) shows that the profiles of tips of screws are affected by the radial thermal expansions. The radial displacements on the tips of male and female rotors are about 4 μm.

In this study, the computational times for the compressor performance, rotor temperature distributions, and rotor thermal deformations are about 10 s, 20 s, and 500 s, respectively, with a personal computer (Intel I3-2100 CPU at 3.1GHz). These computational times are reasonably short, which indicates that the numerical design tools and numerical procedures of this work are efficient and suitable for parametric studies, compressor performance optimization, and sensitivity analysis.

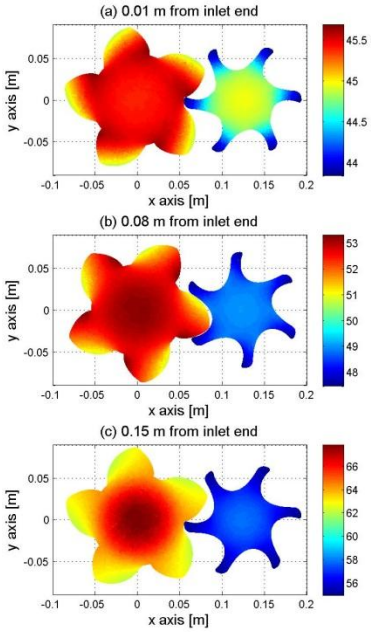

Figure 7: The calculated rotor temperature distributions

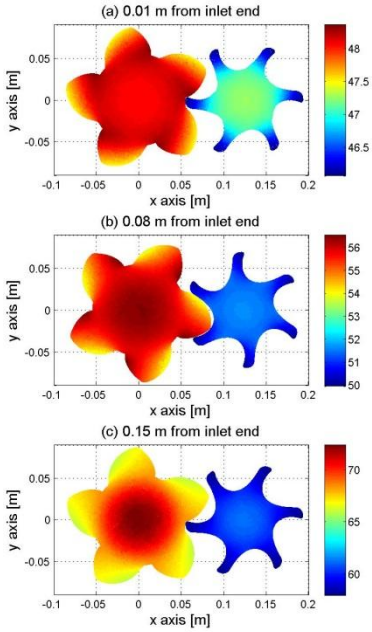

Figure 8: The calculated rotor temperature distributions at 110% heat generation from the bearings of the baseline condition

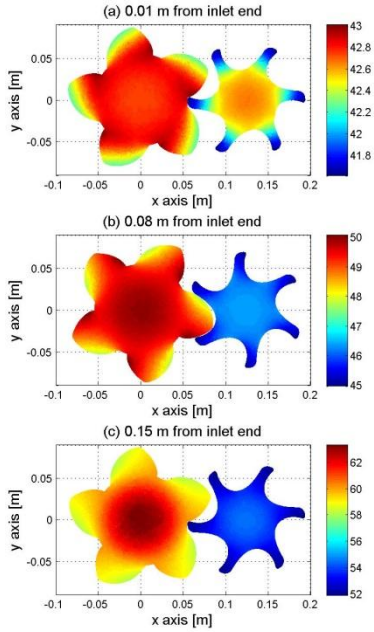

Figure 9: The calculated rotor temperature distributions at 90% heat generation from the bearings of the baseline condition

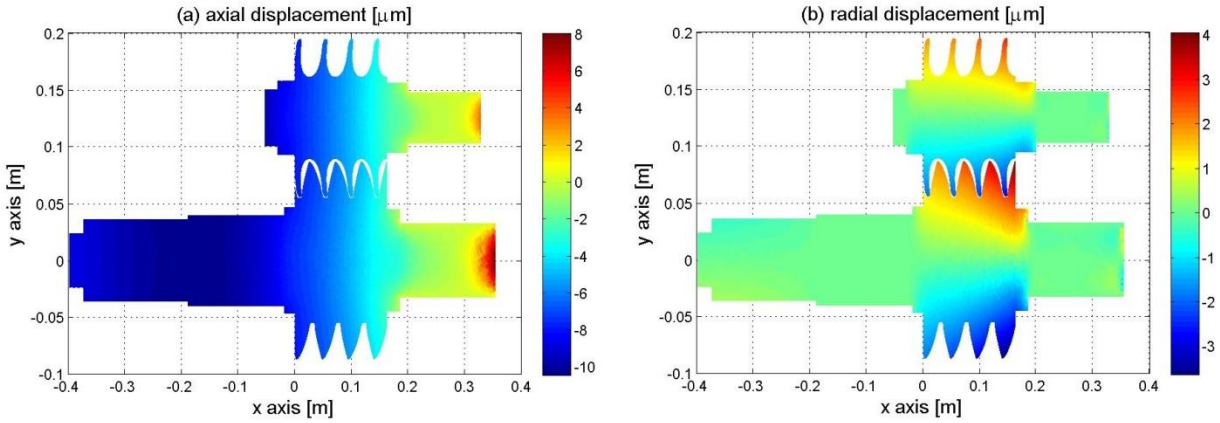

Figure 10: The calculated rotor thermal deformation

4. Conclusion

In this study, numerical design tools are established and integrated to calculate the compressor performance, rotor temperature distributions, and rotor thermal deformations of refrigerant screw compressors. The numerical design tools include lumped parameter analysis for calculating properties of compressed refrigerant, ACE method, for temperature distributions in male and female rotors, and FEM, for thermal deformations of male and female rotors. In the first step, the lumped parameter analysis is implemented to calculate the volumetric and isentropic efficiencies and time variations of pressure and temperature of the compressed refrigerant. The calculated results are then used in the second step, in which the transient three-dimensional heat conduction equation subjected to periodic boundary condition without internal heat generation is solved by the ACE method. The calculated rotor temperature distributions are used in the third step, in which the commercial FEM program, COMSOL Multiphysics (COMSOL),

is used to calculate thermal deformation of male and female rotors. These numerical procedures are completely integrated to efficiently calculate the performance, rotor temperature distributions, and rotor thermal deformations of a refrigerant screw compressor. The numerical design tools are noted to be efficient and suitable for parametric studies, compressor performance optimization, and sensitivity analysis.

NOMENCLATURE

A	area	(m^2)	$T_{reference}$	reference temperature	(K)
A_m	the amplitude	(–)	U	the internal energy	(J)
d_m	bearing pitch diameter	(m)	V	the flow velocity	(m/s)
D	diameter	(m)	$\dot{W}$	the work	(W)
D_H	hydraulic diameter	(m)	**Greek symbols**		
D_o	outer diameter of the screw	(m)	α	thermal diffusivity	(m^2/s)
f	friction factor		α_{th}	the coefficient of thermal expansion	(m/K)
F_{aixal}	average axial load on the bearing	(N)	δ_d	clearance of the outlet end of the screw	(m)
F_{radial}	average radial load on the bearing	(N)	δ_f	clearance of the sealing line of the screw	(m)
h	Heat-transfer coefficient	$(W/(m^2 \cdot K))$	δ_s	clearance of the inlet end of the screw	(m)
$\dot{H}$	the rate of change of enthalpy	(J/s)	ε	roughness	(m)
k	heat capacity ratio		ϵ_{th}	thermal deformation	(m)
L	the length	(m)	μ	dynamic viscosity	$((N \cdot s)/m^2)$
M	the summation of the torques	$(N \cdot m)$	ξ	empirical constant	(–)
Ma_{th}	Mach number	(–)	τ	time in a period	(s)
M_f	torque due to roller end-ring flange sliding friction	$(N \cdot m)$	ψ_m	the space function	(–)
M_l	torque due to applied load	$(N \cdot m)$	θ	the compression angle	(Degree)
M_v	torque due to lubricant viscous friction	$(N \cdot m)$	ω	rotational speed	$(degree/s)$
m	the mass	(kg)	λ	heat conductivity	$(W/(m \cdot K))$
$\dot{m}$	the mass flow rate	(kg/s)	ν	kinematic viscosity	(m^2/s)
n	the unit vector normal to the boundary surface	(–)	ω_m	the frequency	(Hz)
Nu	Nusselt number	(–)	ρ	the density of refrigerant	(kg/m^3)
Nu_D	Nusselt number for pipe flow	(–)	**Subscripts**		
P_r	Prandtl number	(–)	b	bearing	
$\dot{q}_a$	heat flux of unit area	(W/m^2)	bs	bearing on the inlet shaft of the rotor	
$\dot{Q}$	the rate of heat transfer	(W)	bd	bearing on the outlet shaft of the rotor	
r	radial distance	(m)	dis	discharge	
$rem(\ )$	reminder	(–)	ent	entrance	
Re	Reynolds number	(–)	$ideal$	ideal condition	
Re_ω	rotational Reynolds number	(–)	mix	mixed fluid	
Re_D	Reynolds number for pipe flow	(–)	os	oil in the clearance of the inlet end of the screw	
$Re(\ )$	the real part of a complex number	(–)	od	oil in the clearance of the outlet end of the screw	
t	the marching time	(s)	of	oil in the clearance of the sealing line of the screw	

t_p	time period	(s)	oil	oil
T	temperature	(K)	r	rotor
T_d	the auxiliary temperature	(K)	ref	refrigerant

REFERENCES

COMSOL, I., *COMSOL Multiphysics*, http://www.comsol.com/.

Fleming, J. S., Tang, Y., 1995, The analysis of leakage in a twin-screw compressor and Its application to performance improvement, *P I Mech Eng E-J Pro*, vol. 209, no. E2: p. 125-136.

Fleming, J. S., Tang, Y., Cook, G., 1998, The twin helical screw compressor Part 2: a mathematical model of the working process, *P I Mech Eng C-J Mec*, vol. 212, no. 5: p. 369-380.

Fujiwara, M., Osada, Y., 1995, Performance analysis of an oil-injected screw compressor and its application, *Int J Refrig*, vol. 18, no. 4: p. 220-227.

Gao, T. Y., Yang, D. F., Cao, F., Jiao, J. C., 2011, Temperature and thermodynamic deformation analysis of the rotors on a twin screw multiphase pump with high gas volume fractions, *J. Zhejiang Univ.-SCI A*, vol. 12, no. 9: p. 720-730.

Hsieh, S.-H., Shih, Y. C., Hsieh, W.-H., Lin, F.-Y., Tsai, M. J., 2011, Performance analysis of screw compressors – Numerical simulation and experimental verification, *Proceedings of the Institution of Mechanical Engineers, Part C: Journal of Mechanical Engineering Science*, vol. no. p.

Hsieh, S. H., Shih, Y. C., Hsieh, W. H., Lin, F. Y., Tsai, M. J., 2011, Calculation of temperature distributions in the rotors of oil-injected screw compressors, *International Journal of Thermal Sciences*, vol. 50, no. 7: p. 1271-1284.

Jeng, Y. R., Huang, P. Y., 2003, Predictions of temperature rise for ball bearings, *Tribology Transactions*, vol. 46, no. 1: p. 49-56.

Kovacevic, A., 2005, Boundary adaptation in grid generation for CFD analysis of screw compressors, *International Journal for Numerical Methods in Engineering*, vol. 64, no. 3: p. 401-426.

Kovacevic, A., Stosic, N., Mujic, E., Smith, I. K., 2007, CFD integrated design of screw compressors, *Engineering Applications of Computational Fluid Mechanics*, vol. 1, no. 2: p. 96-108.

Kovacevic, A., Stosic, N., Smith, I. K., 2007, *Screw compressors - Three dimensional computational fluid dynamics and solid fluid interaction*, Springer - Verlag Berlin Heidelberg, New York, pp.

Lee, W. S., Ma, R. H., Wu, W. F., Chen, S. L., 1999, Performance and bearing load analysis of a twin screw air compressor, *Chinese Journal of Mechanics-Series A*, vol. 15, no. 2: p. 69-78.

Li, J. F., Wu, H. G., Wang, B. M., Xing, Z. W., Shu, P. C., 2009, Research on the performance of water-injection twin screw compressor, *Applied Thermal Engineering*, vol. 29, no. 16: p. 3401-3408.

Seshaiah, N., Ghosh, S. K., Sahoo, R. K., Sarangi, S. K., 2007, Mathematical modeling of the working cycle of oil injected rotary twin screw compressor, *Applied Thermal Engineering*, vol. 27, no. 1: p. 145-155.

Stosic, N., Hanjalic, K., Kovacevic, A., Koprivica, J., Marijanovic, Z., 1990, Mathematical modeling and experimental investigation of refrigeration screw compressor working process, *Strojarstvo*, vol. 32, no. 1: p. 17-25.

Stosic, N., Milutinovic, L., Hanjalic, K., Kovacevic, A., 1992, Investigation of the Influence of Oil Injection Upon the Screw Compressor Working Process, *Int J Refrig*, vol. 15, no. 4: p. 206-220.

Stosic, N., Smith, I. K., Kovacevic, A., 2005, *Screw compressors - Mathematical modelling and performance calculation*, Springer-Verlag Berlin Heidelberg, New York, pp.

Tedric, A. H., Michael, N. K., 2006, *Essential concepts of bearing technology*, CRC Press, pp.

Wu, H. G., Xing, Z. W., Shu, P. C., 2004, Theoretical and experimental study on indicator diagram of twin screw refrigeration compressor, *Int J Refrig*, vol. 27, no. 4: p. 331-338.

Wu, Y. R., Fong, Z. H., 2008, Rotor profile design for the twin-screw compressor based on the normal-rack generation method, *Journal of Mechanical Design*, vol. 130, no. 4: p. 8.

Xing, Z. W., 2000, *Screw compressors - Theory, dsign and application*, China Machine Press, Beijing, pp. 125-130.

ACKNOWLEDGEMENTS

This paper is supported in part by the National Science Council, Taiwan, ROC (Contract No. NSC 100-2622-E-194-006-CC2).